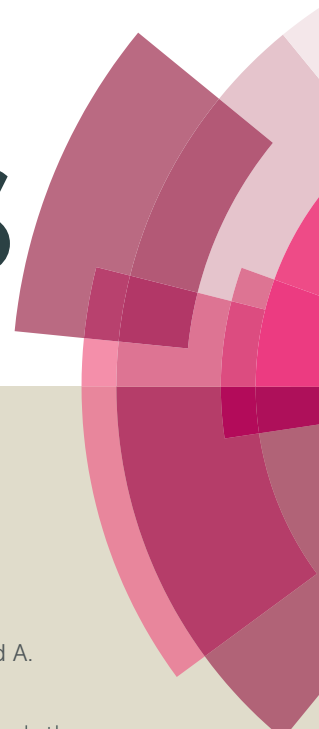


RSC Advances



This article can be cited before page numbers have been issued, to do this please use: E. Tabrizian and A. Amoozadeh, *RSC Adv.*, 2016, DOI: 10.1039/C6RA21048A.



This is an *Accepted Manuscript*, which has been through the Royal Society of Chemistry peer review process and has been accepted for publication.

Accepted Manuscripts are published online shortly after acceptance, before technical editing, formatting and proof reading. Using this free service, authors can make their results available to the community, in citable form, before we publish the edited article. This *Accepted Manuscript* will be replaced by the edited, formatted and paginated article as soon as this is available.

You can find more information about *Accepted Manuscripts* in the [Information for Authors](#).

Please note that technical editing may introduce minor changes to the text and/or graphics, which may alter content. The journal's standard [Terms & Conditions](#) and the [Ethical guidelines](#) still apply. In no event shall the Royal Society of Chemistry be held responsible for any errors or omissions in this *Accepted Manuscript* or any consequences arising from the use of any information it contains.

A new type of SO₃H-functionalized magnetic-titania as a robust magnetically-recoverable solid acid nanocatalyst for multi-component reactions

Elham Tabrizian and Ali Amoozadeh*

Received 00th January 20xx,
Accepted 00th January 20xx

DOI: 10.1039/x0xx00000x

www.rsc.org/

SO₃H-functionalized magnetic-titania nanoparticles (Fe₃O₄@TDI@TiO₂-SO₃H) has been synthesized by a two-step procedure comprising the covalent grafting of n-TiO₂ to n-Fe₃O₄ via 2,4-toluene diisocyanate as a regioselective linker (n-Fe₃O₄@TDI@TiO₂) and subsequent sulfonating by chlorosulfonic acid. The as-prepared nanocatalyst was characterized by Fourier transform infrared spectroscopy (FT-IR), thermogravimetric analysis (TGA), X-ray diffraction (XRD), field emission scanning electron microscopy (FE-SEM) and vibrating sample magnetometer (VSM). The catalytic activity of the nanocatalyst was assessed for synthesis of benzimidazoquinazolinones and polyhydroquinolines, in which the reaction condition was optimized applying central composite design (CCD) through response surface methodology. The nanocatalyst could be separated from reaction mixture easily by magnetic decantation and reused at least six times without a noticeable degradation in catalytic activity. To the best of our knowledge, there are no literature reports on applying experimental design to optimize the reaction condition of benzimidazoquinazolinones synthesis.

1. Introduction

Catalysis is one of the most important fields in the realm of organic synthesis and has been received extensive attention from both academia and industrial points of view¹. Homogeneous Brønsted acid catalysts such as H₂SO₄, H₃PO₄, HF, HCl, HBr, CH₃COOH, CF₃COOH, and *etc.* are widely used in large-scale synthesis of industrial and fine chemicals as well as in organic transformations^{2,3}. Unfortunately, these acids suffer some disadvantages in handling, difficult work-up and separation procedures, waste neutralization and so on. To meet environmental concerns and safety considerations, replacement of corrosive and hazardous mineral acids by heterogeneous ones is one of the main tasks assigned to organic chemists for sustainable production of chemical⁴⁻⁶.

In recent years, extensive deal of attention has been paid to preparation of heterogeneous catalysts by immobilizing homogeneous ones on various solid supports like organic polymers⁷⁻⁹, inorganic silica^{5, 10, 11}, metal oxides¹²⁻¹⁴ and natural supports¹⁵⁻¹⁷. However, this immobilization may usually decreases the selectivity and catalytic activity¹⁸. This drawback can be overcome using nanomaterials as heterogeneous supports. When the size of support is decreased to nanometer-scale, the surface-to-volume ratio is significantly increased, which results in high accessibility of the surface-bound catalytic sites per unit area¹⁹.

Among numerous solid supports, transition-metal oxide nanoparticles have great potential due to their great amount of surface hydroxyl groups that can be used as active sites for the preparation of solid acid catalysts^{20, 21}. Nevertheless, separation of these nanoparticles is almost difficult from reaction mixture by conventional methods²². This problem is surmounted by using magnetic nanoparticle as heterogeneous supports, which can be readily separated employing an external magnetic field, and is typically more effective than centrifugation or filtration as it prevents loss of the catalyst²³⁻²⁶.

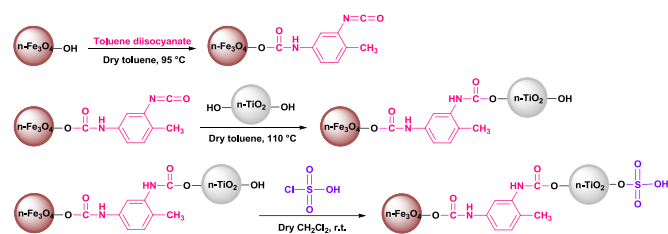
Regarding our researches toward designing and synthesizing novel heterogeneous nanocatalysts for organic reactions^{13, 27-29}, previously, we had reported TiO₂-coated magnetite nanoparticle-supported sulfonic acid as an efficient, magnetically separable heterogeneous solid acid catalyst³⁰ which was prepared through immobilizing SO₃H groups on the surface of Fe₃O₄-TiO₂ core-shell nanostructure. But, very recently, our group uncovered a unique process for magnetization of metal oxides³¹ in which magnetic nanoparticles were bind to nano-titania through the usage of 2,4-toluene diisocyanate (TDI) as covalently linker due to regioselectivity of its two different isocyanate groups. The present developing builds on our prior study to immobilize chlorosulfonic acid on magnetic-titania for preparing non-toxic, low cost, highly efficient, stable, and magnetically recyclable Brønsted solid acid nanocatalyst. The performance of the prepared catalyst was examined in the synthesis of benzimidazoquinazolinones and polyhydroquinolines.

*Department of Organic Chemistry, Faculty of Chemistry, Semnan University, Semnan 35131-19111, Iran; aamozadeh@semnan.ac.ir.

Electronic Supplementary Information (ESI) available: [FT-IR, ¹HNMR and ¹³CNMR spectra]. See DOI: 10.1039/x0xx00000x

2. Result and Discussion

The general synthetic route for the preparation of $\text{Fe}_3\text{O}_4@\text{TDI}@\text{TiO}_2\text{-SO}_3\text{H}$ solid acid nanocatalyst is schematically outlined in Scheme 1. Initially, Fe_3O_4 nanoparticles were prepared by co-precipitation method³². In the second step, Fe_3O_4 nanoparticles were treated with excessive TDI, in which the highly electrophile carbon of the *para*-isocyanate group readily undergo nucleophilic reaction with accessible surface hydroxyls of $n\text{-Fe}_3\text{O}_4$ by forming urethane bond^{33, 34} and preserving the *ortho*-isocyanate group unreacted due to the different reactivity of two isocyanate groups together refer to steric hindrance in TDI³⁵. Subsequently, the as-synthesized nano- TiO_2 ³⁶ was added and in the same way, the surface hydroxyl groups of $n\text{-TiO}_2$ reacted with the preserved *ortho*-isocyanate group of $n\text{-Fe}_3\text{O}_4@\text{TDI}$, in higher temperature and longer reaction time to prepare magnetic-titania. Ultimately, functionalization of the remained surface hydroxyl groups of $n\text{-TiO}_2$ with chlorosulfonic acid led to formation of $\text{Fe}_3\text{O}_4@\text{TDI}@\text{TiO}_2\text{-SO}_3\text{H}$ as a novel type of solid acid nanocatalyst. The catalyst has been characterized by FT-IR, TGA, XRD, FE-SEM, VSM analyses and acid–base titration.



Scheme 1. Preparation of $\text{Fe}_3\text{O}_4@\text{TDI}@\text{TiO}_2\text{-SO}_3\text{H}$ nanocatalyst.

Characterization of $\text{Fe}_3\text{O}_4@\text{TDI}@\text{TiO}_2\text{-SO}_3\text{H}$ nanoparticles

FT-IR spectra

Fourier transform infrared spectroscopy (FT-IR) is one of the effective techniques to characterize the functionalization of nanoparticles. So, FT-IR spectra of every step of the catalyst synthesis is analyzed (Fig. 1). According to our previous report³¹, deposition of TiO_2 nanoparticles on $n\text{-Fe}_3\text{O}_4@\text{TDI}$ is successfully achieved (curve e) due to disappearance of isocyanate peak at 2262 cm^{-1} and the differences in fingerprinting IR bands at the range of $500\text{-}700\text{ cm}^{-1}$ compared to curve d. Immobilization of chlorosulfonic acid on $n\text{-TiO}_2$ surface is verified by the very broad band of acidic group from 2800 to 3500 cm^{-1} and absorption range in $1034\text{-}1267\text{ cm}^{-1}$ which is related to $\text{O}=\text{S}=\text{O}$ asymmetric and symmetric stretching^{13, 29}.

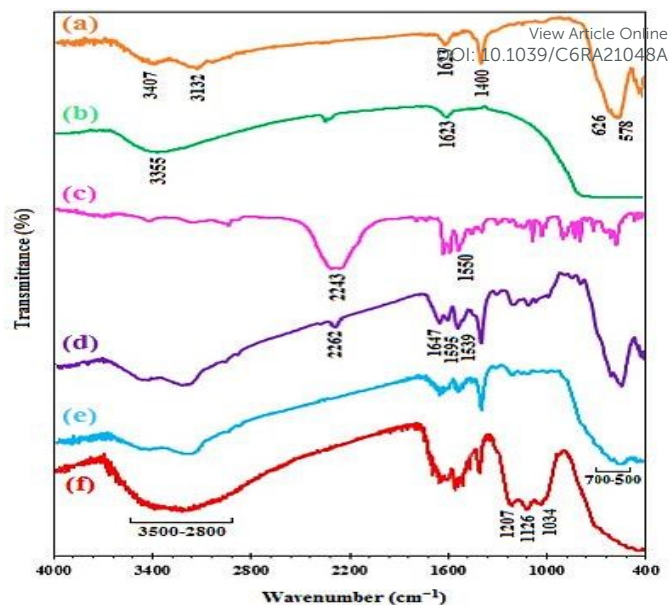


Figure 1. FT-IR spectra of (a) $n\text{-Fe}_3\text{O}_4$, (b) $n\text{-TiO}_2$, (c) TDI, (d) $n\text{-Fe}_3\text{O}_4@\text{TDI}$, (e) $n\text{-Fe}_3\text{O}_4@\text{TDI}@\text{TiO}_2$, (f) $n\text{-Fe}_3\text{O}_4@\text{TDI}@\text{TiO}_2\text{-SO}_3\text{H}$.

Thermo gravimetric analysis

The thermogravimetric analysis (TGA) curve approves grafting of organic groups on the surface of supports by the mass loss of upon heating. As shown in Fig. 2 TGA curves of both $\text{Fe}_3\text{O}_4@\text{TDI}@\text{TiO}_2$ (curve a) and $\text{Fe}_3\text{O}_4@\text{TDI}@\text{TiO}_2\text{-SO}_3\text{H}$ (curve b) are similar, but differs in mass loss amount and temperature range. TGA curve of $\text{Fe}_3\text{O}_4@\text{TDI}@\text{TiO}_2\text{-SO}_3\text{H}$ in the temperature range $30\text{-}800\text{ °C}$ performed three mass losses decomposition. The initial mass loss up to 150 °C is caused by removal of physically trapped solvents and water. The mass loss of about 10.74% between $150\text{-}460\text{ °C}$ and 6.32% between $460\text{-}650\text{ °C}$ is considered to the thermal decomposition of TDI and sulfonic acid groups, which are similar to reported literatures^{13, 37}.

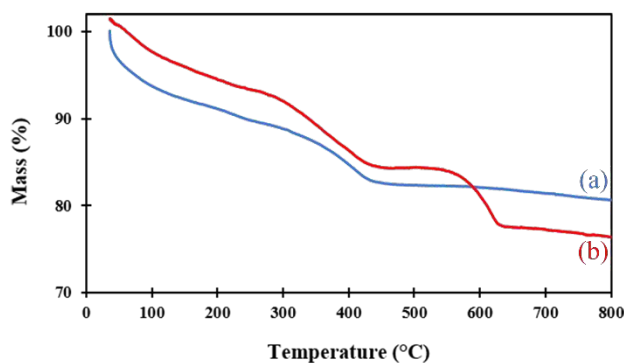


Figure 2. TGA curves of (a) $n\text{-Fe}_3\text{O}_4@\text{TDI}@\text{TiO}_2$, (b) $n\text{-Fe}_3\text{O}_4@\text{TDI}@\text{TiO}_2\text{-SO}_3\text{H}$.

X-ray diffraction spectra

Phase purity and crystal structure of catalyst is analyzed *via* XRD. Cubic Fe_3O_4 structure is confirmed by the peaks at values of 2θ equal to 30.4 (220), 35.7 (311), 43.4 (400), 54.1 (422), 57.1 (511) and 62.9 (440) which is in accordance with JCPD 79-0417, and anatase crystalline phase of TiO_2 is matched with JCPD 89-4921 by the

diffraction signals located at 2θ equal to 25.2 (101), 37.3 (103), 37.8 (004), 38.7 (112), 48.2 (200), 54.0 (105), 55.1 (211), 62.8 (204), 68.9 (116), 70.4 (220), 75.1 (215) and 83.1 (224). The same sets of characteristic peaks of Fe_3O_4 and TiO_2 is detected in the XRD pattern of catalyst (Fig. 3d), indicating that modification is occurred and crystallite phases are retained after treatment by acidic reagent.

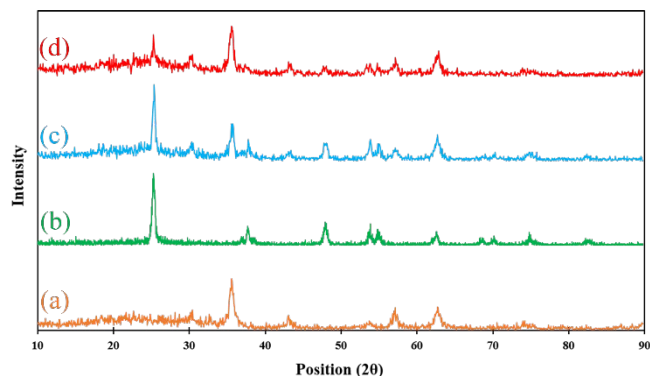


Figure 3. The X-ray diffraction patterns of the (a) $n\text{-Fe}_3\text{O}_4$, (b) $n\text{-TiO}_2$, (c) $n\text{-Fe}_3\text{O}_4@TDI@TiO_2$, (d) $n\text{-Fe}_3\text{O}_4@TDI@TiO_2\text{-SO}_3\text{H}$.

Field emission scanning electron microscopy

Surface morphology, particle shape and size distribution features of $n\text{-Fe}_3\text{O}_4$, $n\text{-TiO}_2$, $n\text{-Fe}_3\text{O}_4@TDI@TiO_2$ and $n\text{-Fe}_3\text{O}_4@TDI@TiO_2\text{-SO}_3\text{H}$ were examined by FE-SEM (Fig. 4). The micrograph illustrate that catalyst particles are quasi-spherical with an enlargement in average diameter size in comparison to that of $n\text{-Fe}_3\text{O}_4$ and $n\text{-TiO}_2$. However, aggregation of the nanoparticles is observed which occurred during functionalization process. The results show the presence of the catalyst in nanometer-sized particles.

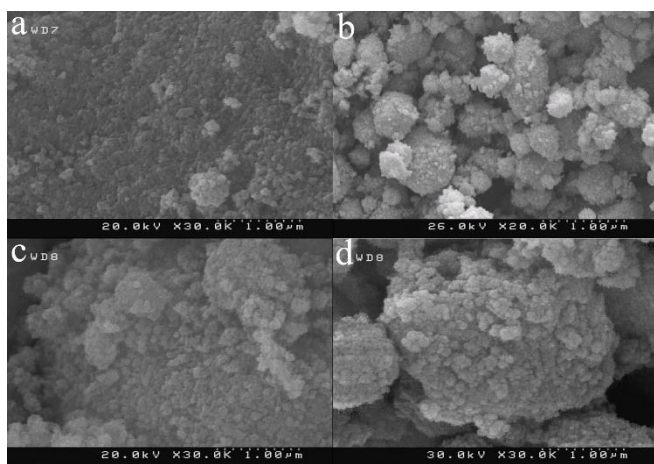


Figure 4. FE-SEM images of (a) $n\text{-Fe}_3\text{O}_4$, (b) $n\text{-TiO}_2$, (c) $n\text{-Fe}_3\text{O}_4@TDI@TiO_2$, (d) $n\text{-Fe}_3\text{O}_4@TDI@TiO_2\text{-SO}_3\text{H}$.

Vibrating sample magnetometer

The magnetic properties of the catalyst was examined at room temperature by using a vibrating sample magnetometer (VSM). The saturation magnetization value of $n\text{-Fe}_3\text{O}_4@TDI@TiO_2\text{-SO}_3\text{H}$ is 31.9 emu/g, lower than that of the bare magnetic nanoparticles (68.4 emu/g) due to presence of non-magnetic layer on the particle surface. Although, this value still reveals its magnetic behavior which

confirms that the magnetization is still large enough for easy catalyst separation by magnetic stirring bar in the reaction mixture.

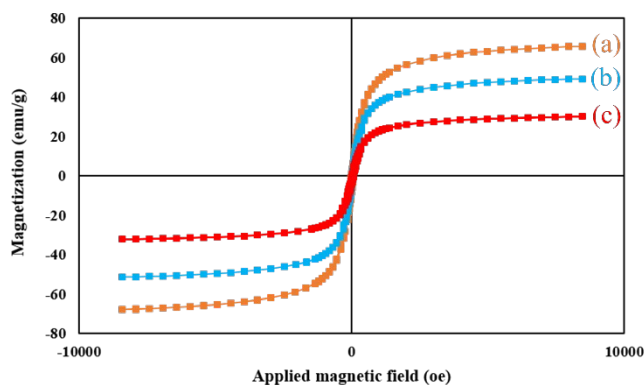


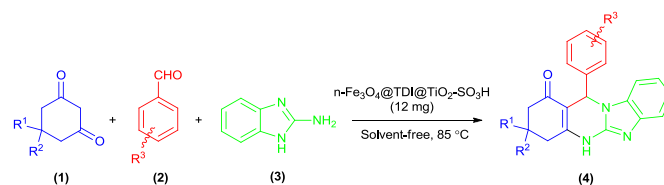
Figure 5. Magnetization curves of the (a) $n\text{-Fe}_3\text{O}_4$, (b) $n\text{-Fe}_3\text{O}_4@TDI@TiO_2$, (c) $n\text{-Fe}_3\text{O}_4@TDI@TiO_2\text{-SO}_3\text{H}$ measured at room temperature.

Acid-base titration

The quantity of sulfonic acid groups on the surface of $n\text{-Fe}_3\text{O}_4@TDI@TiO_2\text{-SO}_3\text{H}$ was determined by ion-exchange pH analysis. To do this, 100 mg of the catalyst was added to 10 mL of a 1 M NaCl solution and stirred continuously for 24 h at room temperature. The catalyst was separated using an external magnet, and the NaCl solution was decanted and saved. Then, two drops of a phenolphthalein solution were added to the NaCl solution and was titrated by 0.01 M NaOH solution to neutrality. According to the obtained results, loading of acid sites was about 2.70 mmol H^+ /g of catalyst.

Evaluating the catalytic activity of $\text{Fe}_3\text{O}_4@TDI@TiO_2\text{-SO}_3\text{H}$ nanoparticles

Nitrogen-containing heterocycles are of considerable interest in the agrochemical and pharmaceutical industries due to diverse range of physiological properties. Benzimidazoquinazolinones, including both biodynamic benzimidazole and quinazoline heterosystems, are an important class of N-heterocycles which possess a broad spectrum of biological activities such as antineoplastic, antihypertensive, anticancer, antihistaminic, anti-HIV, and analgesic properties³⁸⁻⁴⁰. In view of the importance of this heterocycles, performance of $n\text{-Fe}_3\text{O}_4@TDI@TiO_2\text{-SO}_3\text{H}$ as nanocatalyst was probed for the synthesis of benzimidazoquinazolinones *via* condensation between benzaldehyde, dimedone and 2-aminobenzimidazole under solvent-free condition as a model reaction (Scheme 2).



Scheme 2. Synthesis of benzimidazoquinazolinones using $n\text{-Fe}_3\text{O}_4@TDI@TiO_2\text{-SO}_3\text{H}$ as nanocatalyst.

In order to reach the optimal conditions, response surface model (RSM) was employed and effects of catalyst amount (X_1),

ARTICLE

Catalysis Science & Technology

temperature (X_2), and reaction time (X_3) were performed on reaction yield as response. For each factor, 5 levels were defined. These values and their coded are shown in Table 1.

Table 1. Parameter levels and coded values of CCD.

Independent variables	Levels				
	Lowest (-1.68)	Low (-1)	Central (0)	High (+1)	Highest (+1.68)
X_1 : Catalyst amount (mg)	0	5	10	15	20
X_2 : Temperature ($^{\circ}\text{C}$)	30	50	70	90	110
X_3 : Time (min)	4	8	12	16	20

The experimental design matrix and the corresponding experimental parameters and response values are shown in Table 2.

Table 2. Conditions of predicted experiments in CCD.

Run	X_1	X_2	X_3	Yield (%)
1	-1.68	0	0	45.09
2	0	0	0	85.75
3	0	0	0	81.08
4	0	-1.68	0	39.45
5	0	0	+1.68	86.02
6	+1	+1	-1	86.77
7	0	0	0	81.23
8	+1	-1	-1	64.22
9	-1	+1	-1	72.65
10	0	0	0	84.67
11	-1	-1	-1	40.10
12	-1	+1	+1	94.76
13	0	0	-1.68	59.10
14	0	0	0	86.48
15	+1.68	0	0	81.87
16	+1	+1	+1	96.33
17	0	0	0	80.01
18	+1	-1	+1	58.98
19	-1	-1	+1	52.00
20	0	+1.68	0	94.30

The analysis of variance (ANOVA) is used to determine the statistical significance of the constructed models and to evaluate which factor(s) significantly affect the response. From the ANOVA, as shown in Table 3, p-values of model and lack of fit are lower and higher than 0.05, respectively implying that fitted model is significant in confidence level of 95%. Additionally, the results imply that all the independent variables (X_1 , X_2 and X_3) and their quadratic terms (X_1^2 , X_2^2 and X_3^2) significantly affect the response value (yield), and a significant interaction between catalyst amount (X_1) and time (X_3) is obvious ($P < 0.05$). Also, R-squared and adj R-squared amounts are close to 1.0, advocates a high correlation between the observed and the predicted values and indicates that the regression model affords an excellent explanation of the relationship between the independent variables and the response.

Table 3. Analysis of variance for the response surface quadratic model for yield.

Source	Sum of Squares	df	Mean Square	F Value	p-value Prob > F
Model	6247.37	9	694.15	32.50	< 0.0001
X_1 : Catalyst amount	864.33	1	864.33	40.46	< 0.0001
X_2 : Temperature	3788.31	1	3788.31	177.35	< 0.0001
X_3 : Time	511.80	1	511.80	23.96	0.0006

X_1X_2	29.68	1	29.68	1.39	0.2658
X_1X_3	110.19	1	110.19	5.16	0.0465
X_2X_3	78.19	1	78.19	3.66	0.0848
X_1^2	540.19	1	540.19	25.29	0.0005
X_2^2	349.14	1	349.14	16.34	0.0024
X_3^2	122.21	1	122.21	5.72	0.0378
Residual	213.61	10	21.36		
Lack of Fit	175.63	5	35.13	4.63	0.0591
Pure Error	37.97	5	7.59		
Cor Total	6460.97	19			
$R^2 = 0.97$		Adj- $R^2 = 0.94$		Pred- $R^2 = 0.78$	

Polynomial response surface models for yield, based on significant levels and actual values are obtained from the ANOVA:

$$Y (\text{Yield}) = -123.45 + 10.06X_1 + 2.28X_2 + 5.02X_3 - 0.02X_1X_2 - 0.18X_1X_3 + 0.04X_2X_3 - 0.24X_1^2 - 0.01X_2^2 - 0.18X_3^2$$

In this equation, the coefficients show the effect of parameters. Therefore the amount of catalyst can be considered as the main factor in progressing of the reaction.

Response surface plots facilitated the interaction study of process variables on the response by keeping one variable at its zero level and varying the other variables within experimental range. The 3D response plots of yield versus a pair of parameters were applied are shown in Fig. 6. According to their p-values, interaction of X_1X_3 is significant; indicates that simultaneous increment of the catalyst amount and time cause to increase the product yield.

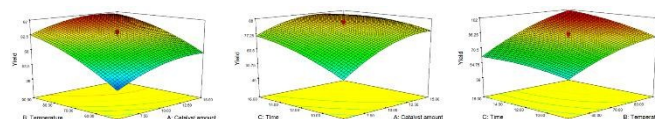


Figure 6. 3-D response surfaces for the effect of factors on the reaction yield.

The main objective of this design is determining the best reaction conditions. Based on the experimental design by using Design-Expert 7.0.0, the model predicted the optimum yield could reach 96.47%, with the optimal process conditions of catalyst amount 12 mg and 85 $^{\circ}\text{C}$ of temperature within reaction time of 13 min.

Currently, with optimum conditions in hand and in order to examine the generality of reaction conditions, the study was extended to different aromatic aldehydes and 1,3-cyclic diketones as shown in Table 4.

Table 4. Synthesis of benzimidazoloquinazolines by $n\text{-Fe}_3\text{O}_4\text{@TDI@TiO}_2\text{-SO}_3\text{H}$.^a

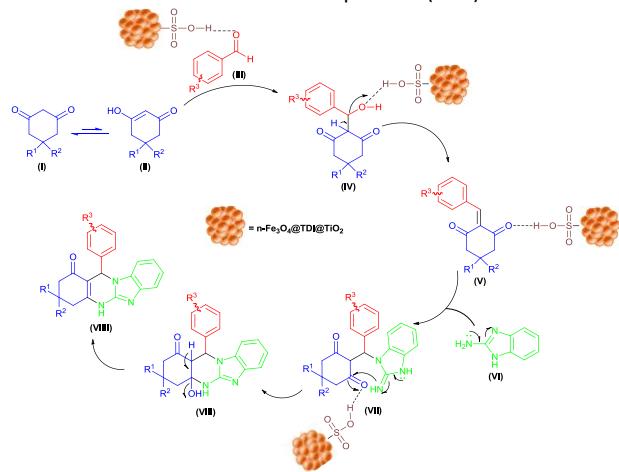
Entry	R ¹	R ²	R ³	Time (min)	Yield ^b (%)	Melting point (°C)
1	CH ₃	CH ₃	-H	13	96	318-320 ⁴¹
2	CH ₃	CH ₃	4-CH ₃	15	91	330-332 ²⁸
3	CH ₃	CH ₃	4-OCH ₃	17	88	317-318 ⁴¹
4	CH ₃	CH ₃	4-OH	15	90	329-331 ⁴¹
5	CH ₃	CH ₃	4-NO ₂	13	92	332-334 ²⁸
6	CH ₃	CH ₃	4-F	12	95	325-326 ²⁸
7	CH ₃	CH ₃	4-Cl	12	91	339-341 ⁴¹
8	CH ₃	CH ₃	4-Br	14	93	314-315 ²⁸
9	CH ₃	CH ₃	4-N(CH ₃) ₂	15	90	>300 ⁴²
10	H	H	-H	15	93	310-312
11	H	H	4-CH ₃	15	90	>300 ³⁹
12	H	H	4-OCH ₃	18	90	>300 ³⁹
13	H	H	4-OH	16	92	>300 ³⁹
14	H	H	4-NO ₂	13	91	>300 ³⁹
15	H	H	4-F	13	94	>300 ³⁹
16	H	H	4-Cl	14	94	>300 ³⁹
17	H	H	4-Br	15	90	>300 ³⁹
18	H	H	4-N(CH ₃) ₂	13	92	>300 ³⁹
19	H	Ph	-H	15	95	332-335 ²⁸

^a Reaction conditions: **1** (1 mmol), **2** (1 mmol), **3** (1 mmol), $\text{Fe}_3\text{O}_4\text{@TDI@TiO}_2\text{-SO}_3\text{H}$ (12 mg) under solvent-free condition at 85 °C.

^b Isolated yield.

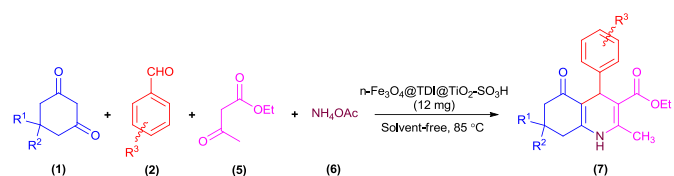
The results illustrate that reaction proceeded very well within relatively short reaction time for 1,3-cyclic diketones and both electron-releasing and electron-withdrawing substituents of aromatic aldehydes, which confirms the high efficiency of the nanocatalyst to a series of structurally diverse benzimidazoloquinazolines in high purity. Formation and purity of products was confirmed by comparing their melting point with the literature values which were in good accordance with them and the structures of some of them were characterized well by using FT-IR, ¹H NMR and ¹³C NMR spectral data.

The suggested mechanism for the synthesis of benzimidazoloquinazolines is patterned in Scheme 3. At the beginning, 1,3-cyclic ketone (**I**) turns to its enol form (**II**) and react with carbonyl group of aldehyde (**III**) which is protonated and activated with the solid acid nanocatalyst and affords (**IV**). Then, α,β -unsaturated carbonyl compound forms upon the loss of water (**V**). Next, α,β -unsaturated carbonyl compound undergoes Michael addition reaction of endocyclic nitrogen in 3-aminobenzimidazole (**VI**), yielding the corresponding intermediate (**VII**). Finally, intramolecular cyclization and loss of water molecule (**VIII**) leads to formation of the desired enamine product (**VIII**).

**Scheme 3.** Probable mechanism for the synthesis of benzimidazoloquinazolines in the presence of $n\text{-Fe}_3\text{O}_4\text{@TDI@TiO}_2\text{-SO}_3\text{H}$.

DOI: 10.1039/C6RA21048A

The promising results mentioned above, encouraged us to extend further the scope of the catalytic performance of $n\text{-Fe}_3\text{O}_4\text{@TDI@TiO}_2\text{-SO}_3\text{H}$ by the synthesis of polyhydroquinolines through the one-pot four-component Hantzsch condensation of 1,3-cyclic diketones, aromatic aldehydes, ethyl acetoacetate and ammonium acetate under the optimized condition reaction of benzimidazoquinazolines (Scheme 4).

**Scheme 4.** Synthesis of polyhydroquinolines using $n\text{-Fe}_3\text{O}_4\text{@TDI@TiO}_2\text{-SO}_3\text{H}$ as nanocatalyst.**Table 5.** Synthesis of polyhydroquinoline derivatives by $n\text{-Fe}_3\text{O}_4\text{@TDI@TiO}_2\text{-SO}_3\text{H}$.^a

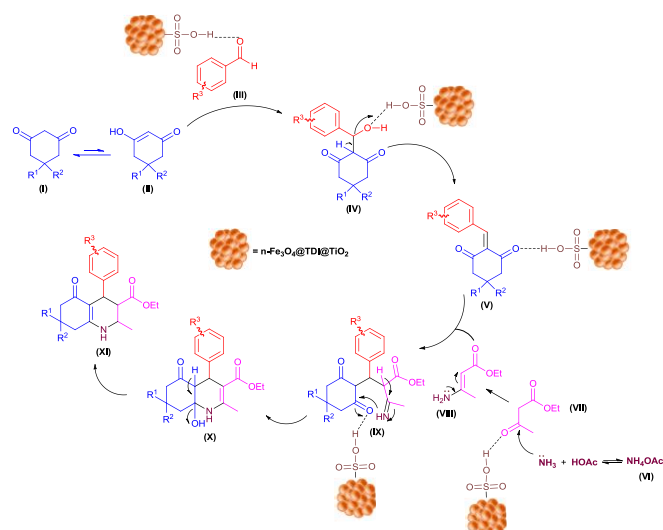
Entry	R ¹	R ²	R ³	Time (min)	Yield ^b (%)	Melting point (°C)
1	CH ₃	CH ₃	-H	15	95	200-202 ⁴³
2	CH ₃	CH ₃	4-CH ₃	16	92	284-286 ⁴⁴
3	CH ₃	CH ₃	4-OCH ₃	18	90	256-258 ⁴³
4	CH ₃	CH ₃	4-OH	18	92	232-235 ⁴³
5	CH ₃	CH ₃	2-NO ₂	18	88	201-203 ⁴⁴
6	CH ₃	CH ₃	3-NO ₂	15	91	170-172 ⁴⁴
7	CH ₃	CH ₃	4-NO ₂	14	94	209-211 ⁴⁴
8	CH ₃	CH ₃	4-F	10	95	181-183 ⁴⁴
9	CH ₃	CH ₃	4-Cl	12	92	245-247 ⁴³
10	H	H	-H	13	94	240-241 ⁴³
11	H	H	4-CH ₃	17	90	240-242 ⁴⁵
12	H	H	4-OCH ₃	16	88	193-194 ⁴⁵
13	H	H	4-OH	20	89	222-223 ⁴⁵
14	H	H	2-NO ₂	20	90	189-191 ⁴⁴
15	H	H	3-NO ₂	15	92	200-202 ⁴⁴
16	H	H	4-NO ₂	12	94	204-205 ⁴⁵
17	H	H	4-F	10	90	243-245 ⁴⁵
18	H	H	4-Cl	10	93	233-234 ⁴⁵
19	H	Ph	-H	18	87	213-214 ⁴⁴

^a Reaction conditions: **1** (1 mmol), **2** (1 mmol), **5** (1 mmol), **6** (2.5 mmol), $n\text{-Fe}_3\text{O}_4\text{@TDI@TiO}_2\text{-SO}_3\text{H}$ (12 mg) under solvent-free condition at 85 °C.

^b Isolated yield.

As shown in Table 5, different aromatic aldehydes bearing electron-withdrawing or electron-releasing substituents and various 1,3-cyclic diketones, gave the desired product in good to excellent yields in short reaction time.

A possible mechanism for the synthesis of polyhydroquinolines is outlined in Scheme 5. First of all, 1,3-cyclic dicarbonyl compound (**I**) converts to its enol form after tautomerisation (**II**) and reacts with carbonyl group of aldehyde which is activated with catalyst (**III**), to afford Knoevenagel intermediate (**V**). On the other side, ammonia resulting from ammonium acetate (**VI**) and the activated β -ketoester by the catalyst (**VII**) yields enamine (**VIII**). Afterward, the reaction between intermediates (**V**) and (**VIII**) gives the intermediate (**IX**). Subsequent tautomerization, intramolecular *N*-cyclization and dehydration yields the hexahydroquinoline.



Scheme 5. Probable mechanism for the synthesis of polyhydroquinolines in the presence of $n\text{-Fe}_3\text{O}_4\text{@TDI@TiO}_2\text{-SO}_3\text{H}$.

To highlight the advantages and effectiveness of prepared catalyst, a comparison of its catalytic activity with some previous methods is presented (Table 6). It approves $n\text{-Fe}_3\text{O}_4\text{@TDI@TiO}_2\text{-SO}_3\text{H}$ is more or less superior over mentioned catalytic systems in terms of easy separability, high activity and recyclability, in addition to high yields of product in short reaction time under neat conditions. These results considerably verify high efficiency of the present catalyst.

Table 6. Comparison of $n\text{-Fe}_3\text{O}_4\text{@TDI@TiO}_2\text{-SO}_3\text{H}$ with other reported catalysts in the synthesis of benzimidazoquinazolines.

Entry	Catalyst	Reaction condition	Time (min)	Yield (%)	Ref.
1	I_2 (10 mol %)	$\text{CH}_3\text{CN}/\text{reflux}$	10	85	46
2	$p\text{-TsOH-H}_2\text{O}$ (15 mol %)	$\text{CH}_3\text{CN}/50\text{ }^\circ\text{C}$	25	95	47
3	$[\text{bmim}^+][\text{BF}_4^-]$ (3 mL)	$90\text{ }^\circ\text{C}$	420	86	48
4	Fe-Chitosan (20 mg)	Ethanol/ $40\text{ }^\circ\text{C}$	105	82	49
5	MCM-41- SO_3H (20 mol %)	Ethanol/reflux	30	97	50
6	$n\text{-Fe}_3\text{O}_4\text{@TDI@TiO}_2\text{-SO}_3\text{H}$ (12 mg)	Solvent-free/ $85\text{ }^\circ\text{C}$	13	96	This work

Recycling of the catalyst

In order to develop greener organic synthesis, the capability of recovering and reusing the catalyst should be considered seriously. In other words, the catalyst should be separated from the reaction mixture, and can be reused several times. Therefore, the recoverability of $n\text{-Fe}_3\text{O}_4\text{@TDI@TiO}_2\text{-SO}_3\text{H}$ was investigated for the model reaction of benzimidazoquinazoline. As shown in Fig. 7, the catalyst can be reused at least six times and a conversion of 89% was still attained in the 6th run.

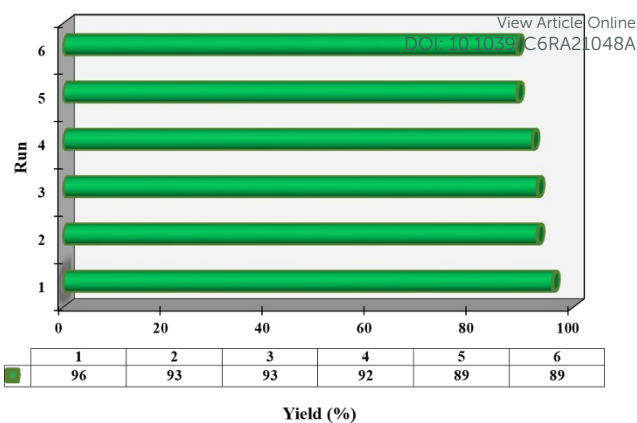


Figure 7. Reusability of $n\text{-Fe}_3\text{O}_4\text{@TDI@TiO}_2\text{-SO}_3\text{H}$ for the synthesis of benzimidazoquinazoline.

After the fifth cycle, the recovered catalyst had similar morphology as the fresh one (Fig. 8) and no noticeable change in structure was observed, by reference to the FT-IR spectrum as compared to the fresh catalyst (Fig. 9)

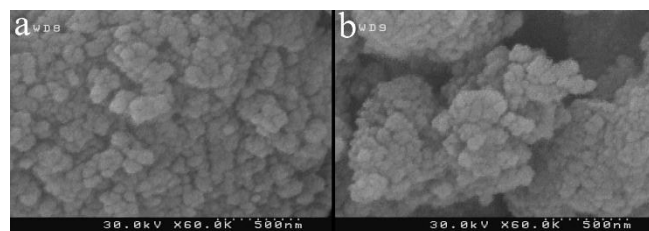


Figure 8. FE-SEM images of (a) fresh $n\text{-Fe}_3\text{O}_4\text{@TDI@TiO}_2\text{-SO}_3\text{H}$, (b) after reused six times.

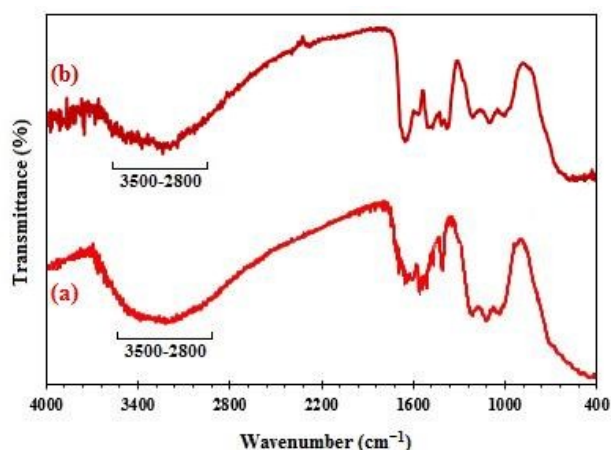


Figure 9. FT-IR spectra of $n\text{-Fe}_3\text{O}_4\text{@TDI@TiO}_2\text{-SO}_3\text{H}$ before use (a) and after reused six times (b).

3. Experimental

Materials and instruments

All chemicals and reagents were purchased commercially from the Aldrich and Merck chemical companies. Solvents were dried by conventional methods. TDI was in industrial grade with 80:20 mixture of 2,4 and 2,6 isomers and was used as received. The progress of the reactions were monitored by thin layer

chromatography (TLC) with silica gel 60 F254 glass plates. Melting points were measured on Thermo scientific 9100 apparatus. FT-IR were recorded on a Shimadzu-8400 spectrometer in the range of 400–4000 cm^{-1} by KBr pellets. Du Pont 2000 thermal analysis apparatus was used for TGA heated from 25 °C to 800 °C with heating rate of 10 °C/min under air atmosphere. XRD patterns were recorded at room temperature on a Siemens D5000 (Siemens AG, Munich, Germany) by Cu-K α radiation. FE-SEM images were performed using a Philips XL30 instrument (Royal Philips Electronics, Amsterdam, The Netherlands) at 30 kV. The magnetite measurement was performed by 4 inch, Daghigheh Meghnatis Kashan Co., Kashan, Iran at room temperature. The NMR spectra were recorded on a Bruker Advance 300 MHz instruments.

Preparation of the magnetic Fe₃O₄ nanoparticles

Magnetic Fe₃O₄ nanoparticles were synthesized by co-precipitation method according to reported literature³². FeCl₃·6H₂O (5.838 g, 0.0216 mol) and FeCl₂·4H₂O (2.147 g, 0.0108 mol) were dissolved in 100 mL deionized water at 80 °C under vigorous stirring and N₂ atmosphere. Then, 25% aqueous ammonia (10 mL) was added into the reaction mixture which resulted in immediate black precipitation of MNPs. After 30 min, the reaction was cooled to room temperature and the precipitate was separated by applying an external magnet, washed several times with distilled water and dried for 48 hr.

Functionalization of Fe₃O₄ nanoparticle with TDI (n-Fe₃O₄@TDI)

Both Fe₃O₄ nanoparticle (1.0 g) and TDI (1.40 g) were dissolved in 50 mL dried toluene by ultrasonic bath for 10–15 min. Next, the reaction mixture was stirred magnetically at 95 °C for 20 h under the atmosphere of nitrogen. Then the powder product was separated magnetically and washed with dry toluene carefully to remove the unreacted and physical absorbed TDI and dried in vacuum at 100 °C for 4 h.

Preparation of TiO₂ nanoparticles

Nano-TiO₂ was synthesized according to the previously reported procedure by hydrothermal method³⁶. NH₃·H₂O was added to solution of TiCl₄ till the pH value reach 1.8. After 2 h stirring at 70 °C, the final solution pH was adjusted to 6 and aged for 24 h at ambient temperature. Then final powder was filtered, rinsed with NH₄Ac-HOAc until no Cl⁻ was perceived. The precipitate was separated by a centrifuge and washed with ethanol, dried in a vacuum. 2 h treatment at 650 °C attained the TiO₂ nanoparticles.

Preparation of the n-Fe₃O₄@TDI@TiO₂

1.0 g n-Fe₃O₄@TDI was dispersed in 100 mL dried toluene. Next, 0.3 g n-TiO₂ was added into and heated at 110 °C for 48 h under constant stirring. The product, n-Fe₃O₄@TDI@TiO₂, was separated by a permanent magnet, washed with acetone and dried at 100 °C for 4 h.

Preparation of the n-Fe₃O₄@TDI@TiO₂-SO₃H

1.0 g Fe₃O₄@TDI@TiO₂ nanoparticles were dispersed in 15 mL dry CH₂Cl₂ and chlorosulfonic acid (0.25 mL, 3.75 mmol) was added drop wisely at room temperature over a period of 30 min. Upon end of the addition, the mixture was continuously stirred for 1 h to allow complete evolution of HCl from the reaction mixture. Then, the solvent was removed under reduced pressure and the powder was

washed three times with ethanol (10 mL) to remove the unattached acids and dried at 100 °C for 5 h.

DOI: 10.1039/C6RA21048A

General procedure for the synthesis of benzimidazoquinazoline derivatives (4)

1,3-cyclic diketone (1 mmol), aromatic aldehyde (1 mmol), 2-aminobenzimidazole (1 mmol) and catalyst (12 mg) were stirred under solvent free condition at 85 °C. Upon completion of reaction (monitored by TLC), the catalyst was separated by applying an external magnet (within 5 s). The reaction mixture was decanted and eluted with hot ethanol (5 mL). The products were obtained by recrystallization of ethanol solution. Percent yields of the products were calculated as follows:

$$\% \text{ yield} = \text{actual yield (g)} / \text{theoretical yield (g)} \times 100$$

General procedure for the synthesis of polyhydroquinoline derivatives (7)

1,3-cyclic diketone (1 mmol), aromatic aldehyde (1 mmol), ethyl acetoacetate (1 mmol), ammonium acetate (2.5 mmol) and catalyst (12 mg) were mixed under neat condition at 85 °C in an oil bath. Upon completion of reaction (monitored by TLC), the catalyst was separated by employing an external magnet (within 5 s). The reaction mixture was decanted and eluted with hot ethanol (5 mL). The products were obtained by recrystallization of ethanol solution. Percent yields of the products were calculated as follows:

$$\% \text{ yield} = \text{actual yield (g)} / \text{theoretical yield (g)} \times 100$$

General procedure for recycling of n-Fe₃O₄@TDI@TiO₂-SO₃H

For evaluating the recoverability of catalyst, the condensation of dimedone (1 mmol), benzaldehyde (1 mmol) and 2-aminobenzimidazole (1 mmol) under the optimized conditions was chosen as model reaction. After completion of the reaction, the catalyst was separated by an external magnet, rinsed thoroughly with ethanol (2 × 5 mL) and acetone (2 × 5 mL), dried at 70 °C for 2 h to be used for subsequent runs.

Conclusions

SO₃H-functionalized magnetic-titania nanoparticles (n-Fe₃O₄@TDI@TiO₂-SO₃H) was successfully synthesized and well characterized by FT-IR, TGA, XRD, FE-SEM, VSM analyses and acid-base titration. FT-IR and TGA confirmed the successful immobilization of sulfonic acid groups. XRD showed crystallinity retention of Fe₃O₄ and TiO₂ nanoparticles after treatment by acidic reagent. FE-SEM results approved nanometer-sized particles of the catalyst and VSM revealed its magnetic behavior for quick magnetic separation with a conventional magnet. Moreover, according to acid-base titration, the sulfonic acid group loading was 2.70 mmol·g⁻¹. The catalyst exhibited excellent activity in the synthesis of benzimidazoquinazolinones and polyhydroquinolines under solvent-free conditions which was optimized by CCD, and affords high to excellent yields of products. Furthermore, the catalyst could be easily separated using an external magnet, and be used repeatedly six times which serves it as an acidic potent heterogeneous nanocatalyst for the chemical transformations.

Acknowledgements

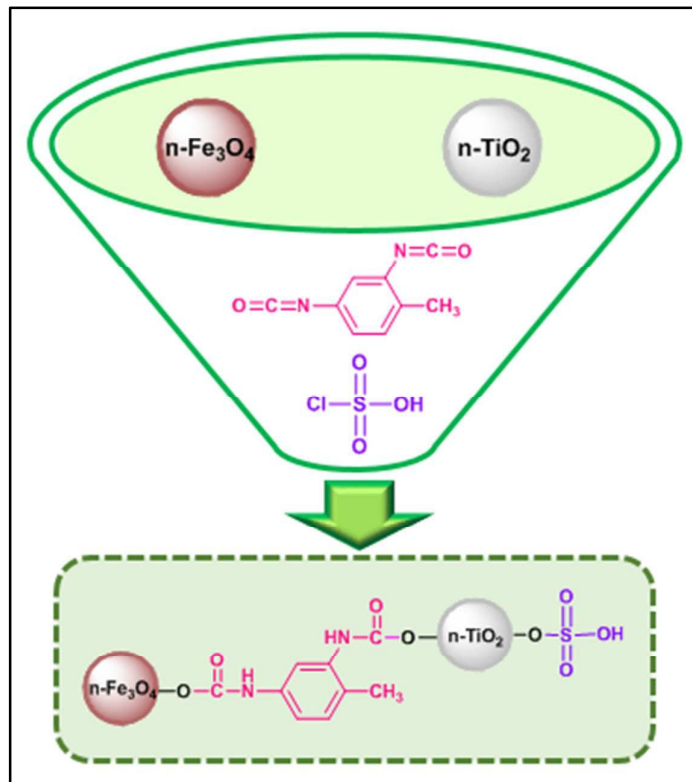
We gratefully acknowledge the Faculty of chemistry of Semnan University for supporting this work.

References

1. A. Corma and H. Garcia, *Adv. Synth. Catal.*, 2006, **348**, 1391-1412.
2. F.-C. Zheng, Q.-W. Chen, L. Hu, N. Yan and X.-K. Kong, *Dalton Trans.*, 2014, **43**, 1220-1227.
3. R. H. Vekariya, K. D. Patel and H. D. Patel, *RSC Adv.*, 2015, **5**, 90819-90837.
4. X. Zhang, Y. Zhao, S. Xu, Y. Yang, J. Liu, Y. Wei and Q. Yang, *Nat. Commun.*, 2014, **5**.
5. M. A. Zolfigol, *Tetrahedron*, 2001, **57**, 9509-9511.
6. J. M. Thomas and W. J. Thomas, *Principles and practice of heterogeneous catalysis*, John Wiley & Sons, 2014.
7. Y. Zhang and S. N. Riduan, *Chem. Soc. Rev.*, 2012, **41**, 2083-2094.
8. P. Puthiaraj and K. Pitchumani, *Green Chem.*, 2014, **16**, 4223-4233.
9. M. M. Heravi, E. Hashemi, Y. S. Beheshtiha, K. Kamjou, M. Toolabi and N. Hosseintash, *J. Mol. Catal. A: Chem.*, 2014, **392**, 173-180.
10. S. Kawamorita, R. Murakami, T. Iwai and M. Sawamura, *J. Am. Chem. Soc.*, 2013, **135**, 2947-2950.
11. H. Naeimi and D. Aghaseydkarimi, *Dalton Trans.*, 2016, **45**, 1243-1253.
12. K. Swapna, S. N. Murthy, M. T. Jyothi and Y. V. D. Nageswar, *Org. Biomol. Chem.*, 2011, **9**, 5978-5988.
13. E. Tabrizian, A. Amoozadeh and S. Rahmani, *RSC Adv.*, 2016, **6**, 21854-21864.
14. M. Hajjami and B. Tahmasbi, *RSC Adv.*, 2015, **5**, 59194-59203.
15. E. Kolvari, N. Koukabi and M. M. Hosseini, *J. Mol. Catal. A: Chem.*, 2015, **397**, 68-75.
16. H. Naeimi and Z. S. Nazifi, *Appl. Catal. A: Gen.*, 2014, **477**, 132-140.
17. G. Ngnie, G. K. Dedzo and C. Detellier, *Dalton Trans.*, 2016, **45**, 9065-9072.
18. A. Ghorbani-Choghamarani and B. Tahmasbi, *New J. Chem.*, 2016, **40**, 1205-1212.
19. E. Lucas, S. Decker, A. Khaleel, A. Seitz, S. Fultz, A. Ponce, W. Li, C. Carnes and K. J. Klabunde, *Chem. – A Eur. J.*, 2001, **7**, 2505-2510.
20. J. Che, Y. Xiao, X. Wang, A. Pan, W. Yuan and X. Wu, *Surf. Coat. Technol.*, 2007, **201**, 4578-4584.
21. R. Ghahremanzadeh, Z. Rashid, A.-H. Zarnani and H. Naeimi, *Dalton Trans.*, 2014, **43**, 15791-15797.
22. N. T. S. Phan and C. W. Jones, *J. Mol. Catal. A: Chem.*, 2006, **253**, 123-131.
23. S. Shylesh, V. Schünemann and W. R. Thiel, *Angew. Chem. Int. Ed.*, 2010, **49**, 3428-3459.
24. Y. Zhu, L. P. Stubbs, F. Ho, R. Liu, C. P. Ship, J. A. Maguire and N. S. Hosmane, *ChemCatChem*, 2010, **2**, 365-374.
25. M. B. Gawande, P. S. Branco and R. S. Varma, *Chem. Soc. Rev.*, 2013, **42**, 3371-3393.
26. F. Nemat, A. Elhampour, H. Farrokhi and M. Bagheri Natanzi, *Catal. Commun.*, 2015, **66**, 15-20.
27. E. Tabrizian, A. Amoozadeh and T. Shamsi, *Reac. Kin. Mech. Catal.*, 2016, **119**, 245-258.
28. A. Amoozadeh and S. Rahmani, *J. Mol. Catal. A: Chemical*, 2015, **306**, 96-107. DOI: 10.1039/C6RA21048A
29. S. Rahmani, A. Amoozadeh and E. Kolvari, *Catal. Commun.*, 2014, **56**, 184-188.
30. A. Amoozadeh, S. Golian and S. Rahmani, *RSC Adv.*, 2015, **5**, 45974-45982.
31. E. Tabrizian and A. Amoozadeh, *Catal. Sci. Technol.*, 2016, **6**, 6267-6276.
32. X. Liu, Z. Ma, J. Xing and H. Liu, *J. Magn. Magn. Mater.*, 2004, **270**, 1-6.
33. H. Xia and M. Song, *J. Mater. Chem.*, 2006, **16**, 1843-1851.
34. Y. S. Chun, K. Ha, Y.-J. Lee, J. S. Lee, H. S. Kim, Y. S. Park and K. B. Yoon, *Chem. Commun.*, 2002, DOI: 10.1039/B205046C, 1846-1847.
35. S. Li and Y. Liu, Polyurethane Adhesive, Chemical Industry Press, Beijing, China, 1998, pp. 13-20.
36. J. Chen, M. Liu, L. Zhang, J. Zhang and L. Jin, *Water Res.*, 2003, **37**, 3815-3820.
37. B. Ou, D. Li, Q. Liu, Z. Zhou and B. Liao, *Mater. Chem. Phys.*, 2012, **135**, 1104-1107.
38. P. Maloo, T. K. Roy, D. M. Sawant, R. T. Pardasani and M. M. Salunkhe, *RSC Adv.*, 2016, **6**, 41897-41906.
39. Q. Shao, S. Tu, C. Li, L. Cao, D. Zhou, B. Jiang, Y. Zhang, W. Hao and Q. Wang, *J. Heterocycl. Chem.*, 2008, **45**, 411-416.
40. M. M. Heravi, L. Ranjbar, F. Derikvand, B. Alimadadi, H. A. Oskooie and F. F. Bamoharram, *Mol. Diver.*, 2008, **12**, 181-185.
41. G. Mohammadi Ziarani, A. Badii, Z. Aslani and N. Lashgari, *Arab. J. Chem.*, 2015, **8**, 54-61.
42. F. Y. a. C. Y. Liqiang Wu, *Bull. Chem. Soc. Ethiop.*, 2010, **14**, 417-423.
43. K. N. Otokesh S, Kolvari E, Amoozadeh A, Malmir M, Azhari S, *S. Afr. J. Chem.*, 2015, **68**, 15-20.
44. A. Amoozadeh, S. Rahmani, M. Bitaraf, F. Bolghan Abadi and E. Tabrizian, *New J. Chem.*, 2016, **40**, 770-780.
45. S. Ko, M. N. V. Sastry, C. i Lin and C.-F. Yao, *Tetrahedron Lett.*, 2005, **46**, 5771-5774.
46. R. G. Puligoundla, S. Karnakanti, R. Bantu, K. Nagaiah, S. B. Kondra and L. Nagarapu, *Tetrahedron Lett.*, 2013, **54**, 2480-2483.
47. M. R. Mousavi and M. T. Maghsoodlou, *Monatsh. Chem.*, 2014, **145**, 1967-1973.
48. C. Yao, S. Lei, C. Wang, T. Li, C. Yu, X. Wang and S. Tu, *J. Heterocycl. Chem.*, 2010, **47**, 26-32.
49. A. Maleki and N. Ghamari, *S. E. C. S.*, 2013, **17**, 1-9.
50. M. R. Naimi-Jamal and M. Karimi, *S. E. C. S.*, 2015, **19**, 1-7.

A new type of SO₃H-functionalized magnetic-titania as a robust magnetically-recoverable solid acid nanocatalyst for multi-component reactions

Elham Tabrizian, Ali Amoozadeh*



This paper highlights a novel synthetic strategy for the preparation of robust and magnetically-recoverable solid acid nanocatalysts.